Microscopic Structure and Binding Mechanism of the Corrosion-Protective Film of Oleylpropanediamine on Copper in Hot Water

Haruka Yoshioka,[†] Ken Yoshida,[*,†] Naoki Noguchi,[†] Tomoyuki Ueki,[†] Kei-ichiro Murai,[†] Kazuya Watanabe,[†,‡] and Masaru Nakahara[§]

[†] Department of Applied Chemistry, Graduate School of Technology, Industrial and Social Sciences, Tokushima University, 2-1, Minamijyousanjima-cho, Tokushima, 770-8506, Japan

[‡] Kurita Water Industries Ltd., 1-1, Kawada, Nogi-machi, Shimotsuga-gun 329-0105, Japan

[§] Institute for Chemical Research, Gokasho, Uji, Kyoto University, 611-0011, Japan

[*] E-mail: yoshida.ken@tokushima-u.ac.jp

ABSTRACT

The structure of the film formed by oleylpropanediamine (OLDA) on the copper (Cu) metal surface in water at 150 °C was investigated by combining quantitative NMR and surface characterization methods. We succeeded in quantifying the amount of film formation by precisely determining all mass balances in the systems examined. 2D IR microscopic mapping showed that the film thickness is uneven in the horizontal direction with a length scale of ~100 μm and hundreds of OLDA layers. This film thickness was also confirmed by AFM. The analysis of the C–H stretching vibrational frequency disclosed that the alkyl chains are highly ordered in the layers close to the Cu surface and are conformationally disordered in the layers distant from the Cu surface in the thicker portion of the film. Combining XPS measurements using argon gas cluster ion beam etching with the ICP-AES analysis, we revealed that the key to multiple layering is the formation of a coordination complex of the unprotonated amino groups of OLDA with Cu that presumably results in polymer chain-like network structures. Contact angle measurements at different OLDA concentrations and treatment times showed that the water repellency of the film originated from the thick layering of OLDA molecules with disordered hydrophobic chains.

INTRODUCTION

The effects of interfacial phenomena of aqueous solution systems at high temperatures are complex and delicate, and a deeper understanding of the surface structure and dynamics is desired in science and engineering. Fundamental studies on interfacial interactions between aqueous systems and metals are essential to improve the safety and efficiency of various containers or pipes under pressure and reduce their maintenance costs. Film-forming amines (FFAs) are a group of organic corrosion inhibitors that have attracted increasing attention for their use in steam–water cycles composed of pressure-resistant materials made of Fe and Cu. FFAs typically have one or two amino groups and a hydrophobic hydrocarbon chain and can form a water-repellent film over a metal surface. The corrosion-protective effects of FFAs have often been attributed to the shielding of the metal surface from the water and vapor phases by the water-repellent film. However, the structure of the film and the mechanism of the film formation have not been clearly understood from the microscopic viewpoint. In this study, we have analyzed the film structure formed on the Cu metal surface in hot water by one of the representative FFAs, oleylpropanedimine (OLDA). Various applications of FFAs and their effectiveness have attracted much attention in the last decade in thermal power plants and various industrial steam generators.[1-4] The circumstances surrounding thermal power generation are shifting to ones that require more frequent shutdowns and layups as a result of the combined use of variable renewable energy. During the shutdowns, corrosion is more susceptible to occur due to oxidation caused by the O_2 uptake and lowering of pH caused by the CO_2 uptake. The use of FFAs is becoming more widespread recently in various industrial steam generators such as those for chemical plants, district heating, and paper production.[5]

The most widely recognized FFAs are the following three species: octadecylamine (ODA), oleylamine (OLA), and OLDA.[2,5] While ODA has been the most widely studied among these three, OLDA has recently received growing interest.[6-9] The existence of two amino groups in OLDA (Figure 1) is expected to enhance its adsorption on metals. Another significant merit of having two amino groups is that it is more suspensible in water than those with one amino group such as ODA and OLA. Recent studies have shown the high adsorption efficiency of OLDA on a stainless steel[6] and its inhibitory effect against flow accelerated corrosion.[7] For practical use of FFAs, there have been some concerns about possible hydrothermal decomposition of FFAs into corrosive organic acids,[2,5,10] however, our recent kinetic research into the supercritical water reaction has shown that decomposed amines produce ammonia, which neutralizes minor byproducts containing organic acids.[11] The high water repellency of the film is often explained as being due to the formation of a monolayer thin film in which the amino groups adsorb on the metal and the hydrophobic groups are directed to water.[12-13] Recently, however, some experimental results have been reported that cannot be explained by the monolayer model, questioning such an oversimplified picture of thin films. For example, the analysis of the adsorption amount has shown that it is on the order of 0.1–1 g m^{-2},[6] which is contradictory to the calculation that it would be on the order of 1 mg m^{-2} for monolayers. On the other hand, Baux et al. concluded that FFAs form a very thin layer of less than 10 nm on the basis of the metal signals in X-ray photoelectron spectroscopy (XPS).[14] Recently, Liu et al. observed the distribution of elements at the cross section of a steel plate using energy-dispersive X-ray spectroscopy and reported that ODA forms a multi-layered film.[15] It is therefore controversial what kind of structure the FFA film forms when it exerts its protective function. Hence, we have carried out experiments combining accurate mass balance (MB) measurement and

surface analysis in order to obtain clear evidence for the formation mechanism and the microscopic structure of the film formed by FFAs.

The objective of this study is to quantitatively analyze the film structure using an approach that combines quantitative analysis of adsorption by solution NMR and surface characterization methods. The sealed tube method allows us to perform experiments under high-temperature and high-pressure conditions in a reaction vessel made of inert materials to confirm the MB.[11, 16-17] Reflection-absorption infrared (RA-IR) microscopy can observe the distribution of an adsorbed amount in the lateral directions with high sensitivity on the order of a micrometer.[18-19] The water repellency of the film was evaluated by the contact angle measurement. The film thickness and the nano-scale morphology of the film surface were examined using atomic force microscopy (AFM) in combination with XPS and the argon gas cluster ion beam (Ar-GCIB) etching method.

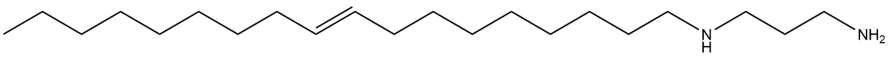

Figure 1. Molecular structure of OLDA.

EXPERIMENTAL SECTION

Copper plates (0.3 mm thickness, 99.96% Cu) were obtained from Nilaco and were cut to 5 × 40 mm pieces. Oleylpropanediamine [N1-(9Z)-9-Octadecen-1-yl-1,3-propanediamine, OLDA, ≥98.0%] was obtained from Amatek Chemical Co. Ltd. Deuterated water (D_2O, 99.9% D, ISOTEC) was obtained from Sigma-Aldrich. The regents and solvents were used without further purification. Most of the adsorption experiments were carried out in D_2O to avoid overwhelming solvent signals in ^1H NMR experiments and to improve the signal-to-noise ratio of OLDA signals,

but some experiments were also carried out in H_2O to check the detectability of N–H vibrational bands in the IR measurements. The solvent H_2O for this purpose was purified using a Milli-Q Gradient A-10 system (Merck Millipore). The aqueous solution of OLDA was prepared at 10 mM (M = mol dm^{-3}) at 45 °C by stirring for more than 6 h. This solution and its diluted solution were used for the adsorption experiments. A Cu plate and 2.0 mL of an OLDA solution were placed in a borosilicate glass tube vessel (6.0 mm i.d. and 8.0 mm o.d.), the air in the gaseous phase was exchanged with argon so that the reaction can be free from O_2 from the air, and the tube was sealed with a gas burner. A high-temperature treatment was carried out by putting the vessel into an electronic furnace preheated to a reaction temperature of 150 °C; the temperature was controlled within ± 1 °C. After a reaction time, the vessel tube was taken out of the electric furnace and put into a water bath to quench the reaction.

The amount of adsorption was analyzed by quantitative ^{1}H NMR measurements using a JEOL ECZ400S spectrometer. After the high-temperature treatment, the solute OLDA molecules initially in the aqueous phase were partitioned into those remaining in the aqueous phase, those adsorbed on the copper plate surface, and those adsorbed on the inner wall of the glass vessel. The concentration of OLDA in the aqueous phase was determined by measuring the concentration of the solution diluted 10 times with deuterated dimethyl sulfoxide (DMSO-d_6) (99.9% D, ISOTEC, Sigma-Aldrich). The purpose of the dilution is to obtain sharper ^{1}H NMR signals, which would be otherwise broadened probably due to the formation of aggregates of OLDA in water at room temperature. The amounts of adsorbed OLDA on the Cu plate and on the inner wall of the vessel were determined from the concentration of the solution in $CDCl_3$ (99.80% D, 0.03% TMS, Eurisotop) made by dissolving the adsorbed OLDA by pouring $CDCl_3$ over the Cu plate or the glass. We checked the MB values defined as MB = $[n_{aq}(t) + n_{Cu}(t) + n_v(t)]/ n_{aq}(0)$, where $n_{aq}(0)$ and

$n_{aq}(t)$ are the amount of OLDA dissolved in the aqueous phase at times 0 and t, respectively, $n_{Cu}(t)$ is the amount of OLDA comprising the film on the Cu plate at time t, and $n_v(t)$ is the amount of OLDA adsorbed on the inner wall of the glass vessel at time t. We found that all OLDA was transferred into the $CDCl_3$ solution with this method by confirming the MB determined using quantitative NMR as demonstrated in Results and Discussion. Furthermore, no IR signal of OLDA was detected after $CDCl_3$ was applied, confirming that no OLDA remained on the Cu plate. We also confirmed that the adhesion of OLDA to the inner surface of the glass tube at ambient temperature can be safely neglected compared to the adhesion at 150 °C. The results of the time course of the OLDA concentration in aqueous solution up to 49 days are shown in Figure S1. The ^{1}H NMR signal was accumulated 16–32 times for the OLDA solutions in a D_2O–DMSO-d_6 mixture and $CDCl_3$. A DSS-d_6 standard solution (500 mg dm^{-3} sodium 3-(trimethylsilyl)-1-propanesulfonate, FUJIFILM Wako Pure Chemicals) was used as an external reference for the integral intensity of ^{1}H NMR signals. DANTE presaturation was used to suppress the ^{1}H signal of impurity HDO.[20] Treatment of the OLDA solution in hot water without a Cu plate was also performed as a reference.

Two-dimensional RA-IR mapping was conducted using a JASCO FT/IR 4600 spectrometer and an IRT-5200 microscope to analyze the surface of the Cu plate taken out of the vessel by opening the glass tube after the high-temperature treatment. RA-IR spectra were measured at 2 cm^{-1} resolution with a JASCO FT/IR 4600 spectrometer equipped with a liquid-nitrogen-cooled HgCdTe detector. IR light was focused on the surface of the Cu plate using a JASCO IRT-5200 microscope equipped with a 10 × Cassegrain mirror. The numerical aperture was set to 0.45, which corresponds to the incidence angle of 26.7°. The polarization condition was in a partially polarized state.[21] As discussed below in the section of Results and Discussion, the

effect of this partial polarization does not affect the quantitative scientific discussion because the dominant OLDA molecules constituting the film can be considered unoriented. The area dimension of the IR mapping was 600 × 600 μm^2, composed of grids of 60 × 60 μm^2. The spectra for each grid were accumulated for 16–64 times to achieve a sufficient signal-to-noise ratio. Reference spectra were measured by using a pristine Cu plate. The integral absorbance of the antisymmetric C–H stretching vibration (2918–2926 cm^{-1}), which is the strongest among those assigned to OLDA, was used to quantify the local amount of OLDA.

The RA was converted to the number of molecules per unit area based on the adsorbed amount determined by quantitative NMR. The RA per area was determined by averaging the IR mapping results at five different locations, each of which covers 600 × 600 μm^2 with 100 grids (i.e., totally 500 grids), on the Cu plate. The amount of OLDA per area on the Cu plate was determined by dividing $n_{Cu}(t)$ by the surface area of the Cu plate. In this way, we established a correspondence between RA per area and the amount of OLDA adsorbed per area, which allowed us to convert RA to the adsorbed amount of OLDA.

To analyze the fraction of elements in the film, we applied XPS. The spectra were acquired using a photoelectron spectrometer (PHI5000 VersaProbe II, ULVAC-PHI) with monochromated Al-Kα radiation (1486.6 eV) at a power of 25 W. We also observed the spectra at regular intervals during Ar-GCIB irradiation. The acceleration voltage of the Ar-GCIB was set to 10 kV since damage to the sample can be satisfactorily suppressed at this voltage. The peaks of Cu $2p_{3/2}$, C 1s, N 1s, and O 1s were measured at a pass energy of 46.95 eV and a step size of 0.1 eV. All spectra are referenced to the C 1s peak at 284.8 eV.

AFM measurements were performed to observe the thickness and surface roughness of the OLDA film. The apparatus used in this study was Hitachi High-Tech AFM5500M and the data acquisition of each point of the height profile was done in the dynamic force mode (DFM).

We examined the Cu content in the film using inductively coupled plasma atomic emission spectroscopy (ICP-AES). To prepare the sample solution for the ICP-AES measurements, the film formed on the Cu plate was solubilized in an aqueous solution using the acid decomposition method. First, the Cu plate on which OLDA adsorbed was taken out of the glass vessel after high-temperature treatment and the plate was rinsed with chloroform so that the film was completely dissolved in the chloroform. The chloroform solution was poured into a beaker, followed by gentle heating of the beaker on a hot plate to evaporate the solvent chloroform. After the OLDA film containing Cu was exsiccated at the bottom of the beaker, a two-fold diluted of concentrated nitric acid (specific gravity = 1.38, Nacalai Tesque Inc.) was poured into the beaker. The beaker was then heated at 90 °C for 1 h, being covered with a watch glass. The solution was then diluted with purified water for the ICP-AES measurement until the nitric acid concentration became less than 0.4 M. The ICP-AES measurements were performed using SPS3520UV from SII NanoTechnology Inc. The signal intensities of Cu were calibrated using a Cu standard solution (100 ppm Cu at 20 °C, Nacalai Tesque Inc.) and its dilution down to 0.1 ppm. The wavelength of 324.754 nm was used for the determination of the Cu content. The spectral acquisitions were done three times for each sample and the standard solution for calibration.

Water contact angle measurements were conducted to assess the hydrophobicity of the film formed on Cu plates. They were carried out using a contact angle meter B100 (Asumi Giken) in combination with SurfScan software (Asumi Giken). Contact angles were measured on the plates

after drying, and five droplets of pure water (0.5 μL) were analyzed at different positions on each plate.

RESULTS AND DISCUSSION

Quantitative NMR Measurement of Adsorption. Let us first examine the formation of the film by means of quantitative NMR measurement of the adsorption of OLDA on a Cu plate. The amount of OLDA observed at each location after 48-h treatment in hot water at 150 °C is shown in Figure 2 together with that in the reference experiment without the Cu plate. When the Cu plate was present, about 20% of OLDA was adsorbed on the Cu plate with ~10% remaining in the aqueous phase. Whereas a large portion (~50%) of OLDA also adheres to the inner surface of the glass tube vessel containing the Cu plate, this amount is much less than that (~90%) in the reference experiment without the Cu plate. The adsorption of OLDA on Cu is considered to have reached saturation within 16 h as the adsorbed fraction of OLDA was already ~30% at 16 h (Figure S2). The amount of OLDA adsorbed on the glass increased from 75% to 90% from 16 h to 48 h, which is found to be saturated later than the adsorption on Cu. These results show that OLDA does preferentially adsorb on the Cu plate, even though the adsorption of OLDA on Cu is competitive with that on the glass. It was also confirmed that the MB was maintained within 15% from 100% at 48 h. The deficit of this magnitude in the MB is presumed to be the formation of aggregates that cannot be observed by the solution-state NMR. In the case of 16-h treatment, the MB is kept constant; the slightly higher value than 100% is considered to be due to the experimental uncertainties. These results on the MB verify that the amount of OLDA adsorbed on the Cu plate is determined with sufficient accuracy for the subsequent discussion.

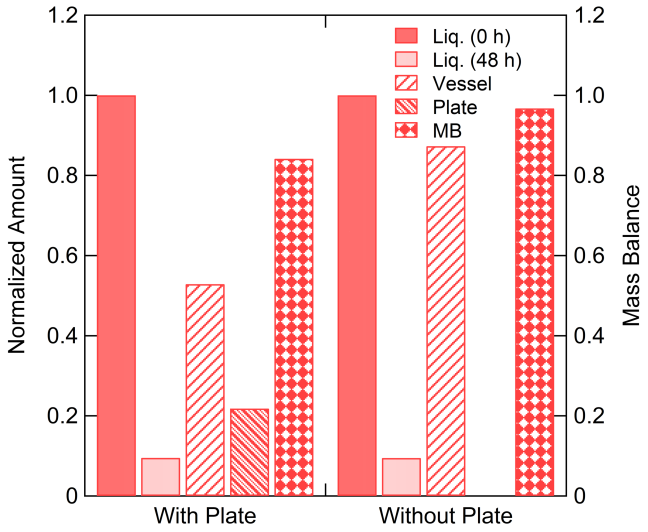

Figure 2. Amount of OLDA observed at each location after 48-h treatment in hot water in adsorption experiments at 150 °C. The vertical axis on the left shows the amount normalized to the initial one in the aqueous phase, and that on the right shows the MB. The normalized amount denotes the amount of OLDA at each indicated position divided by the initial amount.

Adsorption Thickness and Ordered/Disordered Film Structure. Now we discuss the distribution of OLDA adsorbed on the Cu surface based on RA-IR measurements. Figure 3 shows the IR spectra for representative thick and thin film areas obtained using the IR microscopic method; spectra for other areas with intermediate thickness are shown in Figure S3. The integral intensity of the antisymmetric C–H stretching vibration, whose peak position is at 2918–2926 cm^{-1}, was used to quantify the local amount of OLDA. The distribution of OLDA thus obtained is mapped in Figure 4. The most interesting feature is a large unevenness in the distribution. The number of adsorbed OLDA molecules per 1 nm^2 area of the Cu plate (n_A) is in the range of orders of magnitude from 10^2 to 10^3. The formation of thick areas can be due to the high capability of OLDA to assemble on the Cu surface. Meanwhile, even in thin areas, the amount of adsorption is

sufficient to form multiple layers rather than a monolayer. The average n_A value over the Cu plate is 7.7×10^2. This value corresponds to an average film thickness to be 0.5 μm, if we assume that the density of OLDA in the film is the same as that of liquid neat OLDA in ambient conditions (0.84 g cm^{-3}). The thickness is confirmed to be consistent with the AFM measurement combined with Ar-GCIB as demonstrated later.

To grasp the microscopic picture of the stacking OLDA molecules forming the film, it is beneficial to evaluate the film thickness in terms of the number of molecular layers. To convert the n_A value into the number of OLDA layers, it is necessary to assume the dimensions of an OLDA molecule when it is in the film. As shown below, we can safely conclude that the number of layers is of the order of 10^2 on average, regardless of how we assume the shape of an OLDA molecule for the estimation. One of the simplest models is to assume that an OLDA molecule occupies the cubic space. Such a simple model is actually more realistic than one might expect, because we found that the alkyl chains of OLDA are significantly randomized as we shall discuss later. Based on the density of neat liquid OLDA in an ambient condition, the length of one side of the OLDA molecule, assumed to be a cube, is equal to 0.86 nm. This leads to the average number of OLDA layers to be 5.7×10^2. When the OLDA molecule is modeled to be rectangular that is long in one direction, and that the average cross-sectional area σ of the hydrophilic group of OLDA is assumed to be 0.3 nm^2 as a rough estimation, the longest side is calculated to be 2.1 nm. Liu et al. assumed the σ value of ODA to be 0.23 nm^2,[15] and the value we employed for OLDA was set to be larger than that for ODA by taking into account the presence of the two amino groups in OLDA. It is known that the σ value for lipids with two alkyl chains is ~0.6 nm^2,[22] so it is reasonable to assume the σ value of 0.3 nm^2 for OLDA having a single alkyl chain. Based on this model, the average number of OLDA layers over the Cu plate is estimated to be 2.3×10^2 if the OLDA

molecules are vertically arranged and 9.0×10^2 if stacked with their hydrophobic chains in parallel to the Cu surface. Based on the same calculation, we can estimate that even the thin part with the n_A value of 10^2 molecules nm^{-2} has a thickness of about 36–142 stacked OLDA molecules. Importantly, there was not a single grid where the OLDA signals were completely undetectable. This must be vital for the film to exhibit a protective effect. As we will discuss later, AFM shows that there are irregularities on the order of tens of μm in the horizontal direction, and XPS indicates that there are small areas of thickness less than 10 nm in the film, but such thin areas were found to be at most 1–2% of the total film area.

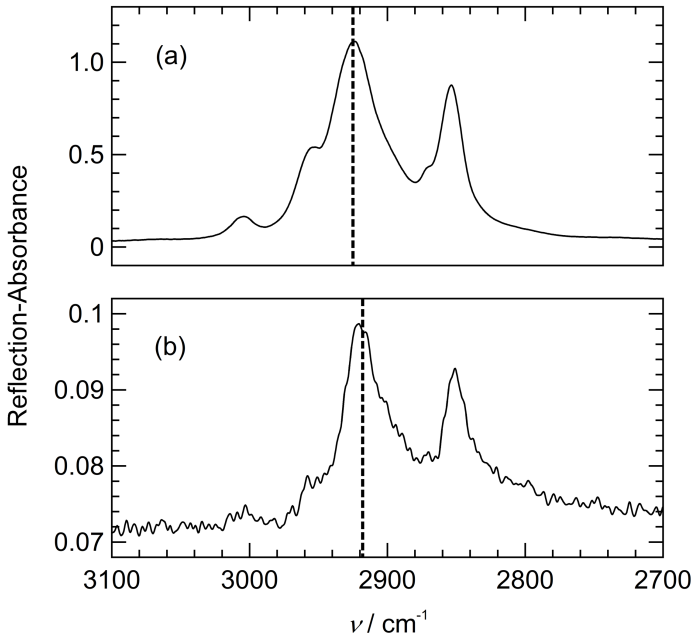

Figure 3. C–H stretching vibration region of the IR spectra of OLDA on a Cu surface after being treated at 150 °C for 48 h in the aqueous phase whose initial OLDA concentration was 1.0 mM. (a) Thick grid (3.3×10^3 molecules nm^{-2}). (b) Thin grid (7.0×10 molecules nm^{-2}).

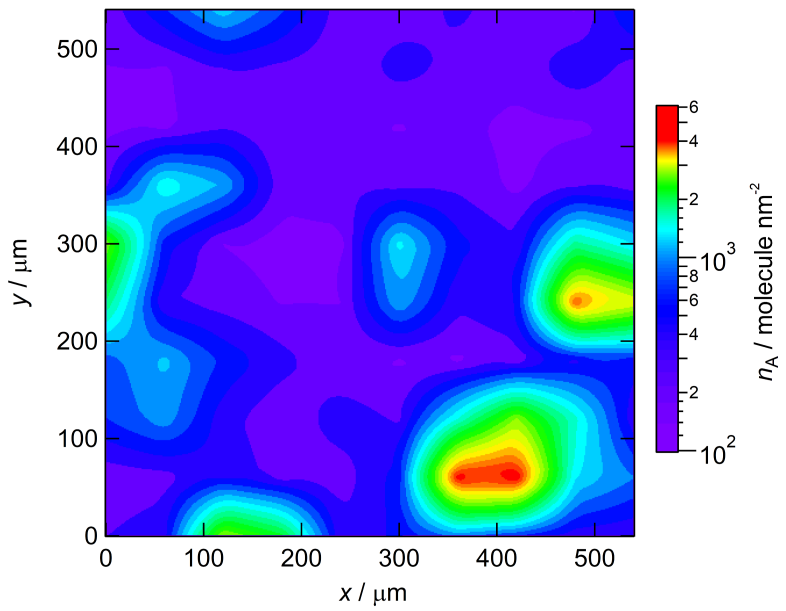

Figure 4. The distribution of the number of adsorbed OLDA per area (n_A) in the horizontal direction along the Cu surface determined using IR microscopy. The temperature, the adsorption time, and the initial concentration of OLDA were 150 °C, 48 h, and 1.0 mM, respectively.

To further scrutinize the structure of the OLDA film on the Cu surface, now let us examine the frequency of the C–H stretching vibration. It has been well established that the frequency of the C–H stretching vibration of alkyl chains is sensitive to the ordered/disordered structure of the alkyl chains.[23-24] When the chains are in all-trans zig-zag conformation and the adjacent chains are packed in an ordered configuration, the frequencies of the antisymmetric ($\nu_{as,CH2}$) and symmetric ($\nu_{s,CH2}$) vibration of the C–H stretching appear at 2918 and 2850 cm^{-1}, respectively. When the chain conformation changes to gauche rotamers, both $\nu_{as,CH2}$ and $\nu_{s,CH2}$ shift to higher frequencies up to 2926 and 2856 cm^{-1}, respectively. It is of great interest to examine if and to what extent the structural ordering varies with the film thickness. In Figure 5, we plot $\nu_{as,CH2}$ against the amount of OLDA adsorbed on the Cu surface; here we chose the one with the higher intensity of the two C–H stretching peaks. A definite tendency is seen for $\nu_{as,CH2}$ to depend on the film thickness. The

value of $\nu_{as,CH2}$ where the film is thin corresponds to the value in the ordered structure. On the other hand, with increasing film thickness, we can see that the ordered structure is lost and shifts to a disordered structure. All OLDA molecules in the first layer directly adhered to the metal surface would have an ordered structure with the amino groups facing the metal side. A similar ordered structure has also been reported for self-assembled monolayers of ODA on mica.[25] A few layers of OLDA close to the first layer are expected to retain the ordered structure because of the structural correlation with the first layer. As the distance from the metal surface increases, the structural correlation with the first layer in direct contact with the metal weakens, and random aggregates are formed by localized association of hydrophilic and hydrophobic groups of the same types. Another contribution to the association of hydrophilic amino groups is likely to be that Cu ions dissolved from the metal penetrate the film and attract the amino groups through coordination bonds. The mechanisms of the film formation based on such inference will be explained in detail later.

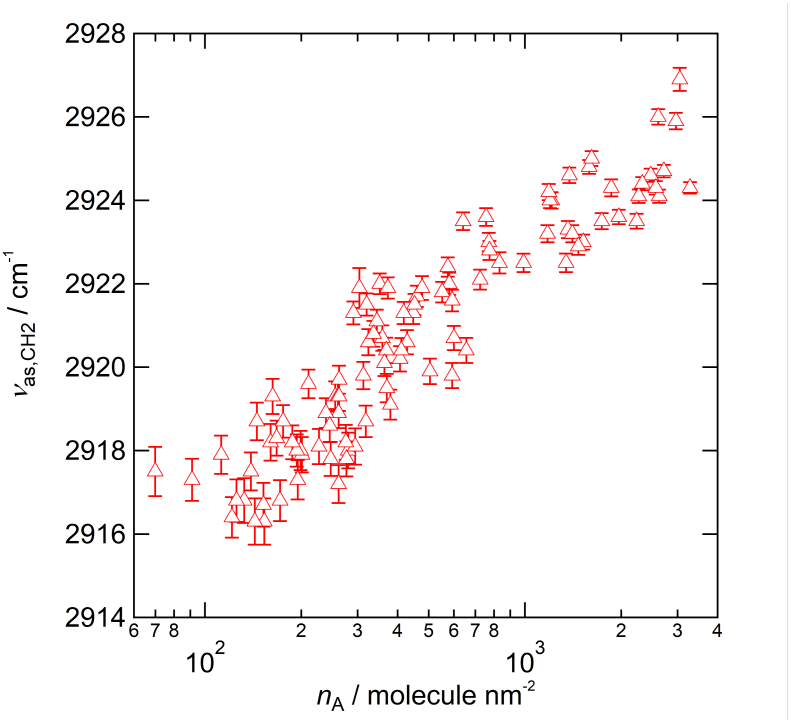

Figure 5. Frequency of antisymmetric C–H stretching vibration ($\nu_{as,CH2}$) plotted as a function of the amount of adsorbed OLDA per area (n_A). The temperature, the adsorption time, and the initial concentration of OLDA were 150 °C, 48 h, and 1.0 mM, respectively.

Now, it is worth mentioning some considerations regarding other amine-related bands. To check whether the N–H stretching band is detectable or not, we measured the IR spectrum of the film formed in H_2O solvent instead of D_2O. For this purpose, we used H_2O because the large C=O stretching band of CO_2 is observed at 2350 cm^{-1}, which is within the range of the N–D stretching vibration (2300–2500 cm^{-1}). There are no such overlapping bands in the region of the N–H stretching vibration (3300–3500 cm^{-1}). We found that the N–H stretching band was not detected in the IR spectrum for the OLDA film, as shown in the spectrum over the whole wavenumber range (Figure S4(a)). The N–D stretching band could not be detected either (Figure S4(b)). This phenomenon has been reported recently by Kuilya et al. that the N–H stretching of ODA is not observed in the case of the film formed with ODA on an incoloy 800 plate.[4] A similar observation

has also been reported recently by Ida et al. for the film formed with a film forming amine product (commercially available products containing a film forming amine as the film forming substance) on a carbon steel plate.[26] The disappearance of the N–H vibrational peak, as also cited and mentioned by Kailya et al, was a common phenomenon observed in the case of ODA and OLA adsorbed on Fe_3O_4 nanoparticles by Pan et al.[27] Importantly, the disappearance of the N–H band is another indicator of complexation, and Pan et al. attributed their undetectability of the N–H band to complexation as well. The detectability of the C–N stretching vibration (~1300 cm^{-1}) could not be checked because its frequency overlaps with the intense P branches of the bending vibration of water vapor (Figure S4). The presence of N atoms in the film was confirmed by XPS, and the absence of observed decomposition products was confirmed by ^1H NMR as described below.

A broad peak at ~3300 cm^{-1}, observed in Figures S4(b), could be assigned to the O–H stretching vibration of water bound to the film. If this is the case, then the water molecules must be forming strong hydrogen bonds, since the wavenumber is smaller than that in liquid water.[28] This is possible because the hydrogen bond distance between amino groups and water is known to be shorter than that between a pair of water molecules.[28] The water molecules are either water entrapped during the formation of the film or water vapor adsorbed after hydrothermal treatment until IR measurement, and the latter is presumed to be predominant. In the case of Figure S4(b), the hydrothermal experiment was performed with D_2O, which means that the H_2O was coming from the water vapor in the air after the sample was removed from the D_2O solution. Although the peak is too broad to discuss the quantitative analysis, its relative intensity to the C–H stretching vibrational band is satisfactorily consistent with the quantitative NMR measurement of water in the film as well as the XPS observation of the O 1s signal as described below.

Here, let us further discuss the reasons why our quantitative IR evaluation is so successful for the film we examine in this study even though our method is based on quite a rough and drastic approximation, assuming the simple proportional correlation between the IR band intensity and the number of molecules. It is known that the orientational dependence of the spectral intensity is of great importance in the IR measurements of films, in particular when the film is very thin and the molecules that comprise the film are highly aligned.[29-30] In the case of the OLDA films observed in this study, on the other hand, we have found that our rough approximation is satisfactorily consistent with the other independent observations by quantitative NMR and AFM. This means that there is not much overall orientational preference of OLDA molecules and this is due to the existence of a quite wide distribution of the direction and the molecular tilting of OLDA. This is highly plausible because the fraction of the OLDA molecules with disordered alkyl chains is overwhelmingly high among those forming the film. In the contour map of the number of stacked OLDA molecules per area based on IR intensities (Figure 4), the area of the thick part of the film might appear to be small. However, if we consider the ratio in terms of the number of molecules that compose the film, the fraction of the thick part is significant; note that the color scale of Figure 4 and the horizontal axis of Figure 5 are both logarithmic. The OLDA molecules that can be grouped in the disordered side, for example, with the antisymmetric C–H stretching vibrational frequency $\nu_{as,CH2}$ above 2921 cm^{-1}, account for ~80% of the total OLDA molecules forming the film; Figure S5 plots the fraction of OLDA molecules whose $\nu_{as,CH2}$ value is less than or equal to ν. We further confirmed that no dramatic change was observed in the spectral shape of $\nu_{as,CH2}$ over a wide range of film thickness as can be seen in Figure S3. The contribution of the disordered OLDA is therefore dominant as found in our evaluation of the relationship between IR intensity and molecular number in combination with NMR results.

Cu-Induced Stacking Mechanism. The NMR and IR observations discussed above indicate that the film is formed by the accumulation of tens or hundreds of multilayers of OLDA molecules. One may ask why such many OLDA molecules can be stacked. Combining XPS measurements using Ar-GCIB etching with ICP-AES analysis, we have succeeded in revealing the indication that the multiple layering is made possible with the coordination complex formed by the unprotonated amino groups of OLDA with Cu ions dissolved from the surface of the Cu plate, which could lead to the polymer-chain-like network structures across the film. To investigate this possibility, we first verified that the film contains a significant amount of Cu atoms. We solubilized the film and ions (if any) in the film by the acid decomposition method as described in the experimental section above and determined the amount of Cu atoms contained in the film using ICP-AES. The number of Cu atoms distributed across the film is thus determined to be 1.3×10^2 atoms per 1 nm^2 on average, which corresponds to the molar ratio of Cu atoms to OLDA molecules of 1:6. The concentration of Cu atoms in the dilute nitric acid solution introduced into the ICP-AES apparatus was 0.2 ppm, which was 2 orders of magnitude higher than the detection limit of the apparatus (several ppb to 10 ppb), so the atomic emission spectrum showed a highly distinct Cu signal. Therefore, there is no doubt that the film contains one Cu atom for every several OLDA molecules. Because the Cu content is this high, it can be assumed that the self-assembly can be extended by forming a configuration that resembles coordination polymers. Moreover, the existence of two amino groups in OLDA may allow OLDA to become a bidentate ligand, or the two amino groups of a single OLDA molecule may coordinate with two different Cu atoms, which can contribute to the extension of the aggregate network. To the best of our knowledge, such a mechanism has never been discussed for aliphatic FFAs, specifically, OLDA, ODA, and OLA.

The formation of a coordination networking structure was demonstrated for an azole-type corrosion inhibitor (5-hexyl-l,2,3-benzotriazole) on Cu examined by combining time-of-flight secondary ion mass spectroscopy and XPS.[31] For imidazole, there is also a report suggesting the formation of a network structure as studied by XPS.[32]

To further examine the states of the elements in the film, we performed XPS analysis of the film formed on the Cu plate in combination with the Ar-GCIB etching method. Figure 6 shows the XPS spectra of C 1s, N 1s, and Cu $2p_{3/2}$ orbitals that are stacked as a function of the etching time. In the spectra of the unetched film, we can clearly see C 1s and N 1s peaks that are attributed to OLDA; the enlarged view of the spectra for the unetched film is shown in Figure S6. The peak of the dominant C 1s signal is observed at the binding energy of the sp^3 hybrid orbital of a carbon atom with C–C bonds (284.8 eV, referenced value). This is reasonable since the signal should be assigned to the carbon atoms of the hydrocarbon chain of OLDA. The peak of the N 1s signal is located at 399.2 eV. This peak is assigned to $–NH_2$ and –NH– residues since the binding energy is close to the $–NH_2$ residue of a functionalized graphene.[33] In the previous examination of imidazole reacted with CuO,[32] the peaks at 398.8 and 399.8 eV are assigned to the N atom forming N–Cu bond and that of the free N–H residue, respectively. The peak observed presently at 399.2 eV is in between these two binding energy values, which means that the state of OLDA in the film is a mixture of those that bind to Cu and those that do not. This is consistent with the presence of 6 times as many OLDA molecules as Cu atoms in the film. In the present results, neither a peak nor a shoulder was observed around 401.8 eV, which corresponds to the binding energy of $–NH_3^+$ and $–NH_2^+–$;[33] see the enlarged spectrum in Figure S6(b). Thus, the amino groups of OLDA in the film are found to be dominantly in the unprotonated, neutral state, rather than in the protonated state. This result further shows that deamination does not occur under the current condition of 150 °C.

The decomposition of amines is so slow that it takes several tens of hours even at 400 °C.[11] The neutral amino residue has lone pair electrons, which is advantageous for not only the adsorption of amino groups on the Cu plate but also the formation of a coordination complex with Cu ions in the film. In the Cu $2p_{3/2}$ region, a small signal can be observed in the unetched state at 932.6 eV (Figure S6(c)). Based on the binding energy value, this signal can be assigned to Cu(0) (932.6 eV).[34]

As the etching proceeds, the signal of C 1s and N 1s decreased, while that of Cu $2p_{3/2}$ increased as can be seen in Figure 6. This is quite natural because OLDA molecules of the film were removed step by step by etching, and the exposed area of the Cu plate became larger. The peak position of Cu $2p_{3/2}$ does not change as the etching proceeds, so this is consistent with the attribution of the Cu signal seen in the pre-etch spectrum to the metallic Cu of the plate. The detection of a Cu signal without etching does not immediately mean that the film thickness is less than 10 nm. The Cu signal can be observed because there is at least a small area of the thin region originating from the Cu plate in the range where the signal is strong enough to exceed the detection limit.

The key is to focus on the ratio of atoms present on the film surface. Figure 7 plots the elemental existence ratios, calculated from the conversion from the XPS signal intensities, against the irradiation time of etching. This figure shows that the fraction of C atoms ceases to decrease when ~15% remains. This can be an observation of the C atoms of OLDA that are so strongly bound to the Cu plate that they cannot be sputtered by the Ar-GCIB. Correspondingly, the increase in Cu will also reach a plateau at about 80%. At the end of 100 min of Ar-GCIB irradiation, it was confirmed by AFM (described below) that the sub-μm level of the raised area of the film had been removed. Before etching, a small amount of oxygen is also observed at about 8% (Figure 7). This

O 1s signal observed at ~531 eV (Figure S7(a)) may have originated from Cu_2O (530.3 eV).[35] There might be some minor contribution of hydroxide ion (531.0 eV) or water (532.8 eV) in the vicinity of the hydrophilic groups;[36] the molar ratio of water to OLDA in the film was determined to be 1:5, which corresponds to the fact that the atomic molar quantity of water oxygen is 1% of OLDA carbon. The O atoms may originate mainly from adsorbed water vapor, as noted above regarding the discussion of IR spectra in Figure S4. This signal was reduced by etching, and the binding energy was shifted to ~532 eV (Figure S7(b)). The remaining oxygen after the etching was ~5% and this may have originated from the strongly-binding water or adsorbed oxygen gas from the air (~533 eV).[37]

To examine whether the Cu-plate-derived signal is shielded when OLDA is applied more thickly, XPS was measured by increasing the initial concentration of OLDA 10-fold to 10 mM. The Cu $2p_{3/2}$ signal before the etching was barely detectable as seen in Figure 8a; however, the binding energy of 933.3 eV for Cu^{2+} is distinguishable from that for the metallic Cu that should appear at 932.6 eV.[34, 37] Taking the molecular structure of OLDA into account, it is most plausible to interpret the peak seen in the unetched case as a Cu^{2+} ion coordinated with an amino group (or groups) of OLDA. To the best of our knowledge, there are no reports on the binding energy of Cu $2p_{3/2}$ for Cu ions coordinated with the amino residues of OLDA. Since the binding energy differs depending on the type of the amino group coordinated, it is rather difficult to conclude what kind of coordination complexes are formed based on the binding energy alone, for example, 932.9 eV (3-aminopropyltri-methoxysilane for modification of montmorillonite),[38] 933.4 eV (tetracycline on a chelating resin),[39] and 936.4 eV (modified polyurea)[40]. Nevertheless, the difference in the binding energy with and without etching clearly proves that the Cu signal from the unetched state originates from the Cu^{2+} ions embedded in the film and cannot be assigned to the metallic Cu of

the plate. The signal of the spectrum acquired after 2-min etching is shifted to 932.6 eV (Figure 8b), which corresponds to the neutral Cu(0) as in the case in which the initial OLDA concentration was 1.0 mM.

Solution NMR observations also indicate that OLDA can form coordination bonds with Cu in the films formed on the Cu surface. We dissolved the film in deuterated chloroform ($CDCl_3$) and measured the ^1H NMR spectrum of this solution. We found that the ^1H signals for the methylene groups that are adjacent to the amino groups (peaks i, j, and l in Figure 9(a)) are broadened to such a level that they cannot be detected presumably because of the complex formation of amino groups with the Cu contained in the film as shown in Figure 9(b). This solution-state observation suggests that complex formation between OLDA and Cu can also occur in the film formed on the Cu plate. A previous solution-state NMR study has shown that the microenvironment of lipids dissolved in chloroform can mimic the states of lipids in bilayer membranes with respect to the association of hydrophilic/hydrophobic groups.[41] Thus, we inferred that OLDA films dissolved in chloroform can reflect the environment inside the film. There are no peaks attributed to degradation products in Figure 9(b). This is also consistent with the XPS results, which showed that deamination did not occur at 150 °C.

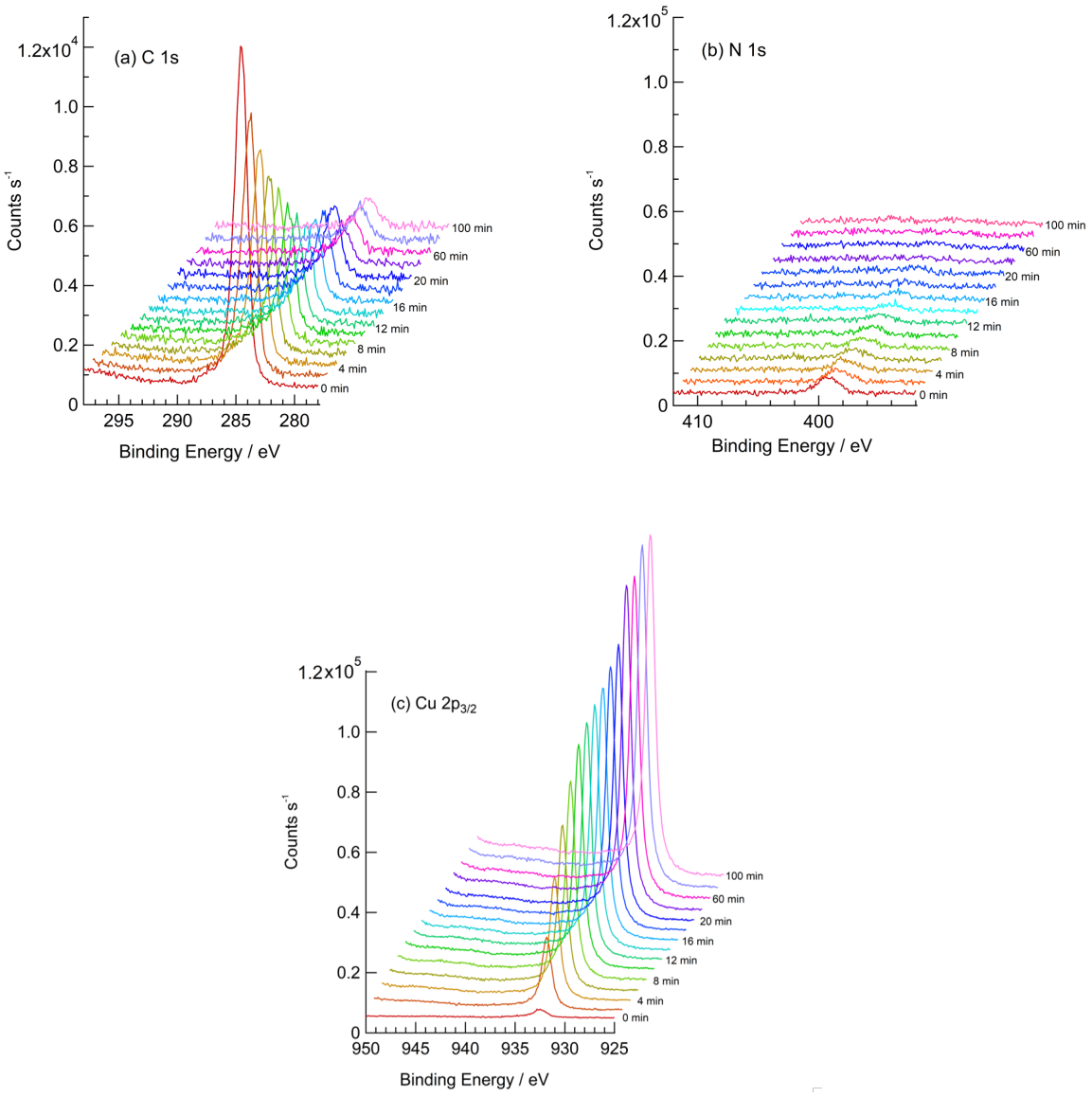

Figure 6. Stack plots of the XPS spectra of (a) C 1s, (b) N 1s, and (c) Cu $2p_{3/2}$ orbitals for the OLDA film stacked as a function of the sputtering time. The temperature, the adsorption time, and the initial concentration of OLDA were 150 °C, 48 h, and 1.0 mM, respectively.

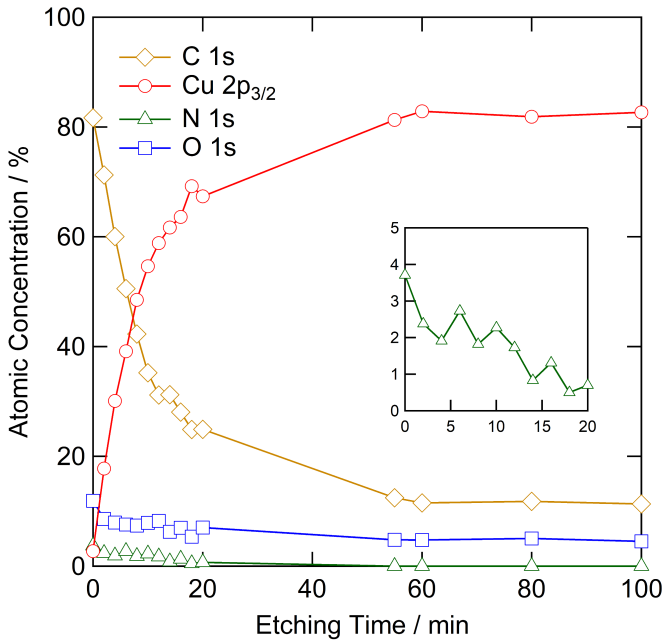

Figure 7. Elemental distribution in the OLDA film as a function of the etching time. The temperature, the adsorption time, and the initial concentration of OLDA were 150 °C, 48 h, and 1.0 mM, respectively. The inset is the enlarged view for the time course of N atoms; the amount of N after 55 min is below the detection limit. The total of C, N, O, and Cu is assumed to be 100% since the amounts of other elements are negligibly small as confirmed in the wide-range spectrum.

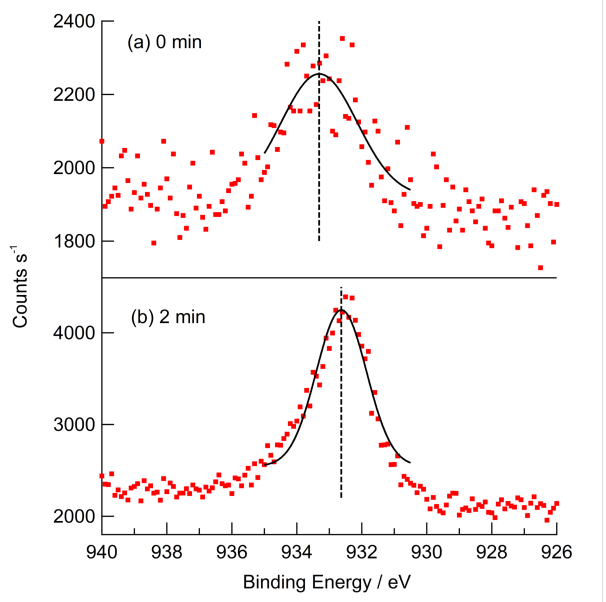

Figure 8. XPS spectra of the Cu $2p_{3/2}$ orbital for (a) the pre-etched OLDA film and (b) that after 2-min etching. The temperature, the adsorption time, and the initial concentration of OLDA were 150 °C, 48 h, and 10.0 mM, respectively.

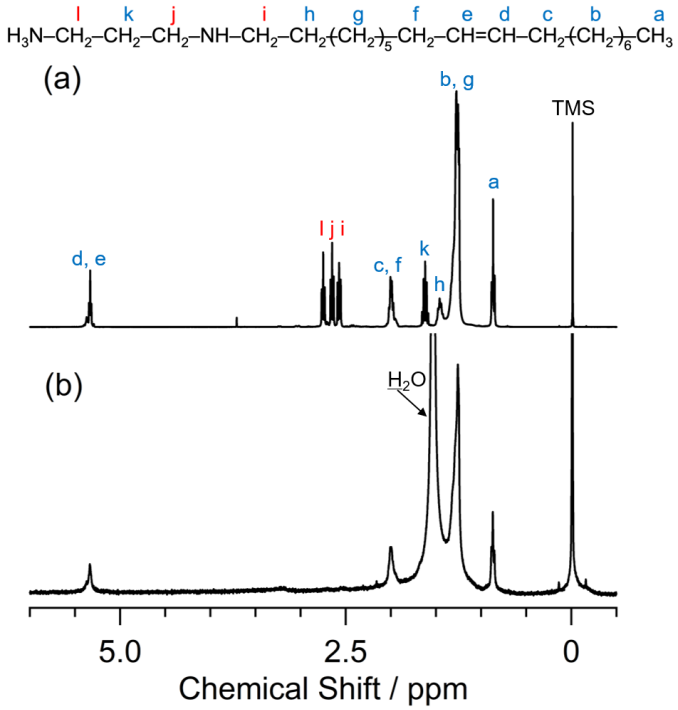

Figure 9. ^{1}H NMR spectrum of (a) OLDA (untreated regent) and (b) the OLDA film formed on the Cu plate dissolved in $CDCl_3$. The temperature, the adsorption time, and the initial concentration of OLDA for (b) were 150 °C, 48 h, and 1.0 mM, respectively.

Surface Morphology and Film Thickness. The nano/micro scale surface structure and thickness of the films were investigated by combining XPS and Ar-GCIB described above with AFM. To directly probe the film thickness, we removed the film by the position-selective etching and attempted to observe the difference in height between the etched and unetched areas by AFM. Etching was conducted by scanning XPS until the distribution of elements observed by XPS plateaued, which meant that the majority of the OLDA molecules at the etched position were

removed (Figure 7). The boundary of the etched area was first recognized by the eye and then qualitatively distinguished in the image using the microscope built into the AFM equipment (Figure 10(a)). A cross-sectional view across the etched/unetched boundary is shown in Figure 10(b); cross sections at different positions are shown in Figure S8. The etched portion has a roughly constant height with fine irregularities, while the unetched portion has a gentle rise with a smooth surface. The filmed part is convex or concave in the horizontal (parallel to the plane) direction with an interval of several tens of μm, and on average the height of the filmed part was confirmed to be higher than that of the exposed Cu plate. For the quantitative determination of the thickness of the film, the average thickness of the film was evaluated as the average height over the film area. The average thickness of the film thus determined was 0.4 μm. This is in surprisingly good agreement with the film thickness estimated by analyzing the IR signal intensities based on the amount of adsorbed OLDA determined by quantitative NMR.

Here let us discuss the water repellency of the film surface often referred to in the practical application. An important feature observed for the films in relation to water repellency is the presence of sharp edges on the film surface as can be seen noticeably in Figures S8(b) and S8(d). From the nano-scale point of view, we note here that the water repellency of the OLDA film originates from the so-called lotus effect in addition to the hydrophobicity of the hydrocarbon chains. An essential feature of the film is that it has nano-/micro-scale irregularities, rather than the flat monolayer planes often assumed previously.[12-13] These irregularities will be advantageous for improving the evaporation efficiency in boilers. Topp et al. have previously reported that FFA coating enhances the heat transfer coefficient of a pool boiler.[42] The surface irregularities of the film found here are considered to have the effect of increasing the evaporation efficiency of the

boiler by advantaging the nucleation of bubbles and the release of the formed bubbles from the surface.

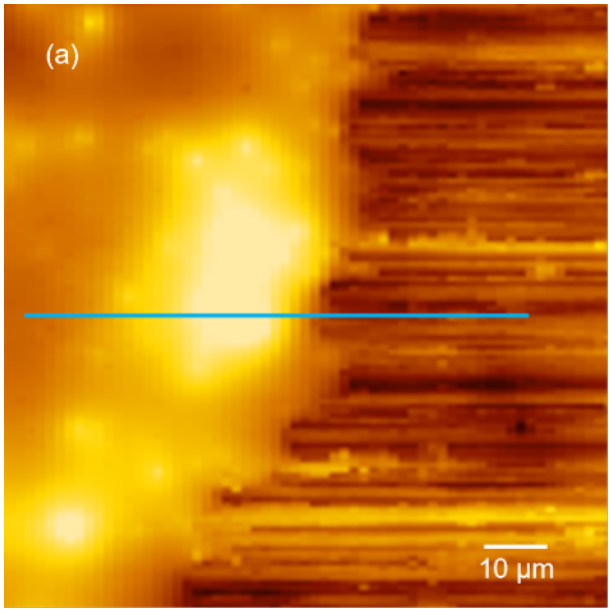

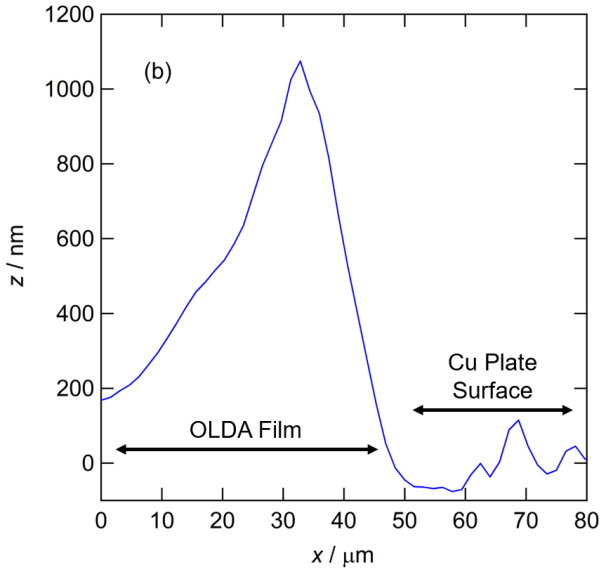

Figure 10. (a) AFM 2D image of a Cu plate coated with the OLDA film after 100-min of etching and (b) a typical cross-sectional plot of the AFM result across the boundary between the etched and unetched area. The sliced position for (b) is indicated by the blue horizontal line in (a). The temperature, the adsorption time, and the initial concentration of OLDA were 150 °C, 48 h, and 1.0 mM, respectively.

Water Contact Angle. To macroscopically examine the hydrophobicity of the film at the interface with the aqueous phase, we measured the water contact angle of the OLDA film formed on the Cu plate. The measurements were performed for different initial OLDA concentrations and hot-water treatment times, and the results are summarized in Table 1. The average contact angles at different treatment times were almost the same. On the other hand, the variation of the contact angle with locations was greatly affected by the treatment time, and the distribution, represented by the standard deviation of the contact angle values at different positions, was significantly reduced at 48 h to about one-third of the value at 16 h for both the initial concentrations of 1.0 and 10.0 mM. In other words, the treatment time increased the uniformity on a macroscopic scale on the order of millimeters.

When the initial OLDA concentration was changed, the average contact angle was about 15–20° larger at 10.0 mM than that at 1.0 mM. Since the IR results show that the film fully covers the Cu plate, the contact angle reflects the ratio of hydrophobic to hydrophilic groups exposed on the upper surface of the film. The mechanism of the pronounced concentration effect found here can be given from the microscopic viewpoint as follows. At low concentrations, the transfer of micellar or unimolecular OLDA in the aqueous phase to the film occurs more independently; NMR and IR results show that the film is composed of multiple layers, and it is natural that the OLDA at the top surface is oriented with its hydrophilic group toward the aqueous phase to achieve the energetically stable configuration. At high concentrations, OLDA is in a more crowded state in the

aqueous phase. During the time that the OLDA in the aqueous phase approaches the surface of the film and settles into an energetically stable optimal structure, it will be collided by another OLDA molecule that is successively supplied from the aqueous phase to the film. In such a situation, a relatively random metastable structure is expected to be built up with some hydrophilic groups bound together inside the film, and accordingly, the OLDA molecules at the interface can orient their hydrophobic tails toward the aqueous phase. In this regard, water repellency is not necessarily required for the purpose of corrosion prevention by shielding the metal surface from the aqueous phase. In the thin part of the film, the alkyl chains are aligned, so that the high ordering can prevent water from penetrating the film and initiating corrosion. In the thick part, on the other hand, the structure of the film is randomized, but its sufficient thickness between the aqueous phase and the metal surface can hinder the water penetration. In the case where imparting water repellency to a metal surface is an objective in itself (e.g., improving thermal conductivity through dropwise condensation[43]), it is beneficial to pay attention to the concentration of the aqueous phase during the film formation.

Table 1. Water Contact Angle θ at Various Treatment Times t at 150 °C and Initial OLDA Concentrations C_0.[a]

C_0 / mM	t / h	θ / °
1.0	16	74 ± 36
1.0	48	75 ± 10
10.0	16	91 ± 26

10.0	48	97 ± 9

[a] Distributional ranges are shown with 95% confidence limits.

CONCLUSIONS

The present study is the first comprehensive investigation that combined the quantitative evaluation of FFA adsorption with surface characterization. We investigated OLDA as an FFA, whose possession of two amino groups is expected to enhance both aqueous suspensibility and adsorption on metals. A quantitative evaluation of the amount of adsorption and film thickness was achieved by solution NMR. We succeeded in identifying all locations where OLDA was transferred in hot water: adsorbed on the Cu plate, remaining in aqueous solution, or otherwise adsorbed on the inner surface of the glass vessel. Based on the amount of OLDA adsorbed on the Cu plate, which was accurately determined by such an NMR approach, the film was found to consist of tens or hundreds of layers. The thickness of the layer estimated in this NMR method (0.5 μm) agreed very well with the results of the AFM measurement of the difference in height obtained by removing the OLDA with Ar ion cluster beams until it reached the Cu plate surface (0.4 μm). A film formed to that level of sufficient thickness is likely to be effective in preventing corrosion.

Two-dimensional IR mapping revealed the inhomogeneity of the film thickness in the horizontal direction with a length scale of ~100 μm. From the C–H vibrational frequencies, we found that the OLDA molecules in the thin part were aligned due to the adsorption of amino groups to the Cu plate, and in the thicker part, the configuration of OLDA was more disordered. The AFM measurement detected finer unevenness in the horizontal direction with a length scale of ~10 μm. The concavity and convexity are expected to be advantageous for water repellency. In the case of the application of FFAs to steam generators, the unevenness should facilitate the detachment of

nucleated bubbles, which can be the microscopic origin of the possible benefit of the film to thermal efficiency.

The driving force for the multilayer formation can be explained by the Cu ions dissolved from the Cu plate and embedded in the film. The presence of Cu atoms in the film was evidenced by ICP-AES. The molar amount of Cu in the film was about one-sixth of that of OLDA. Furthermore, ^{1}H NMR observation of the film dissolved in chloroform showed that the methylene proton signals in the vicinity of the amino groups of OLDA were so broadened that almost no peaks were detectable, suggesting the coordination of the amino groups of OLDA with Cu. Such complex formation can enhance the formation of the thick film by stacking of OLDA, presumably owing to polymer chain-like network structures. The orientations of OLDA in the film are randomized due to the attraction of amino groups by Cu ions penetrating the film, except for those in the vicinity of the Cu plate surface where OLDA molecules are aligned in a lamellar pattern as inferred from the IR results. The randomized configuration of OLDA is also considered to be advantageous for water repellency as was observed by contact angle measurements. Since OLDA molecules as well as other FFAs have hydrophobic chains comprising a large portion of their molecules, they can exhibit hydrophobicity when randomized in locations where the film is sufficiently thick. In view of the interaction between the film and the aqueous phase, it is energetically advantageous if the OLDA on the top surface forms hydrogen bonds with water molecules with hydrophilic groups facing the aqueous phase. This situation can only be achieved if the film is thin enough and consists of an even number of layers, and if there is a high correlation between the configuration of OLDA molecules on the aqueous solution side and the Cu plate side. The contact angle measurements disclosed that the larger the amount of OLDA added, the better

the water repellency, and the longer the treatment with hot water, the better the homogeneity of the water repellency across the film.

Future research is needed to systematically investigate the kinetics and equilibrium of film formation, the roles of the different structures of various FFA molecules, and the effects of thermodynamic conditions, such as temperature and FFA concentrations. Such science-based insights will provide great help to develop practical guidelines, which will be increasingly needed to improve the safety and efficiency of water/steam technologies using FFAs.

Supporting Information.

The following files are available free of charge at:
https://pubs.acs.org/doi/10.1021/acs.jpcc.2c00526

Time course of the OLDA concentration in an aqueous solution at room temperature, OLDA amount at different positions with an initial concentration of 10 mM, C–H stretching vibration region of the IR spectra of OLDA on a Cu surface at different locations with various film thicknesses, IR spectra of OLDA on a Cu surface treated in H_2O and D_2O over the whole wavenumber range, fraction of OLDA molecules as a function of the C–H stretching frequency, enlarged view of pre-etched XPS spectra, XPS spectra of the O 1s orbital, and cross-sectional view of AFM results at different positions (PDF).

ACKNOWLEDGMENT

This study is supported by grants-in-aid for Scientific Research (nos. 17H06456, 20K04131, and 20K05433) from the Japan Society for the Promotion of Science (JSPS). K.Y. is also grateful for

the research fund from the Japan Association for the Properties of Water and Steam (JPAPWS). We thank Tokushima Regional Base for Industry-Academia-Government Joint Research for use of the ICP-AES apparatus. Dr. Hitoshi Mizuguchi at Tokushima University is thanked for helpful discussions about ICP-AES measurements. Shintaro Mori, Kazuyoshi Uchida, and Masakazu Koizumi at Kurita Water Industries Ltd., and Nobuo Ishihara at Mitsubishi Heavy Industries Ltd. are thanked for fruitful discussions.

REFERENCES

1. Betova, I.; Bojinov, M.; Saario, T. Film-Forming Amines in Steam/Water Cycles–Structure, Properties, and Influence on Corrosion and Deposition Processes. VTT Technical Research Centre of Finland research report, Vol. VTT-R-03234-14; Department of Information Technology, Lappeenranta University of Technology, Espoo, Finland, 2014.

2. International Association for the Properties of Water and Steam, *Application of Film Forming Substances in Fossil, Combined Cycle, and Biomass Power Plants*, Technical Guidance Document IAPWS TGD8-16, 2019.

3. Hater, W., Film Forming Amines – an Appraisal. PowerPlant Chem. **2021**, 23, 162-175.

4. Kuilya, S.; Subramanian, V.; Bera, S.; Rangarajan, S. Evaluation of Octadecylamine for the Corrosion Inhibition of Incoloy 800. *Corros. Eng. Sci. Tech.* **2021**, *56*, 119-128.

5. International Association for the Properties of Water and Steam, *Application of Film Forming Substances in Industrial Steam Generators*, Technical Guidance Document IAPWS TGD11-19, 2019.

6. Cuoq, F.; Benguigui, J.; Geijselaers, C.; Lampert, F. Linking Thermoelectric Effect and Adsorption of Film Forming Amine as a Corrosion Inhibitor for Industrial Systems. *Ind. Eng. Chem. Res.* **2020**, *59*, 8492-8495.

7. Weerakul, S.; Leaukosol, N.; Lister, D. H.; Mori, S.; Hater, W. Effects on Flow-Accelerated Corrosion of Oleylpropanediamine under Single-Phase Water Conditions Pertinent to Power Plant Feedwater. *Corrosion* **2020**, *76*, 217-230.

8. Xue, Y.; Vughs, D.; Hater, W.; Huiting, H.; Vanoppen, M.; Cornelissen, E.; Verliefde, A.; Brunner, A. M. Liquid Chromatography–High-Resolution Mass Spectrometry-Based Target and Nontarget Screening Methods to Characterize Film-Forming Amine-Treated Steam-Water Systems. *Ind. Eng. Chem. Res.* **2020**, *59*, 22301-22309.

9. Jiang, B.; Sun, W.; Cai, J.; Chen, S.; Hou, B. Inhibition of Carbon Steel Corrosion in Hcl Solution Using N-Oleyl-1,3-Propanediamine Based Formulation. *Colloids Surf. A: Physicochem. Eng. Asp.* **2021**, *624*, 126824.

10. Moed, D. H.; Verliefde, A. R. D.; Rietveld, L. C. Effects of Temperature and Pressure on the Thermolysis of Morpholine, Ethanolamine, Cyclohexylamine, Dimethylamine, and 3-Methoxypropylamine in Superheated Steam. *Ind. Eng. Chem. Res.* **2015**, *54*, 2606-2612.

11. Yoshida, K.; Yoshioka, H.; Ushigusa, N.; Nakahara, M. ^{14}N NMR Evidence for Initial Production of NH_3 Accompanied by Alcohol from the Hydrolysis of Ethylamine and Butylamine in Supercritical Water. *Chem. Lett.* **2021**, *50*, 316-319.

12. Turner, C. W. Fouling of Nuclear Steam Generators: Fundamental Studies, Operating Experience and Remedial Measures Using Chemical Additives. *AECL Nuclear Review* **2013**, *2*, 61-88.

13. Dooley, B.; Lister, D. Flow-Accelerated Corrosion in Steam Generating Plants. PowerPlant Chem. **2018**, *20*, 194-244.

14. Baux, J.; Causse, N.; Esvan, J.; Delaunay, S.; Tireau, J.; Roy, M.; You, D.; Pebere, N. Impedance Analysis of Film-Forming Amines for the Corrosion Protection of a Carbon Steel. *Electrochim. Acta* **2018**, *283*, 9.

15. Liu, C.; Lin, G.; Sun, Y.; Lu, J.; Fang, J.; Yu, C.; Chi, L.; Sun, K. Effect of Octadecylamine Concentration on Adsorption on Carbon Steel Surface. *Nucl. Eng. Technol.* **2020**, *52*, 2394-2401.

16. Yoshida, K.; Wakai, C.; Matubayasi, N.; Nakahara, M. NMR Spectroscopic Evidence for an Intermediate of Formic Acid in the Water−Gas−Shift Reaction. *J. Phys. Chem. A* **2004**, *108*, 7479-7482.

17. Kimura, H.; Hirayama, M.; Yoshida, K.; Uosaki, Y.; Nakahara, M. Effect of Water on Hydrolytic Cleavage of Non-Terminal α-Glycosidic Bonds in Cyclodextrins to Generate Monosaccharides and Their Derivatives in a Dimethyl Sulfoxide–Water Mixture. *J. Phys. Chem. A* **2014**, *118*, 1309-1319.

18. Noguchi, N.; Yonezawa, T.; Yokoi, Y.; Tokunaga, T.; Moriwaki, T.; Ikemoto, Y.; Okamura, H. Infrared and Raman Spectroscopic Study of Methane Clathrate Hydrates at Low Temperatures and High Pressures: Dynamics and Cage Occupancy of Methane. *J. Phys. Chem. C* **2021**, *125*, 189-200.

19. Islam, A.; Abdel-Rahman, M. K.; Trenary, M. Heat of Adsorption of Propyne on Cu(111) from Isotherms Measured by Reflection Absorption Infrared Spectroscopy. *J. Phys. Chem. C* **2021**, *125*, 18786-18791.

20. Morris, G. A.; Freeman, R. Selective Excitation in Fourier Transform Nuclear Magnetic Resonance. *J. Magn. Reson.* **1978**, *29*, 433-462.

21. Shinoda, K.; Aikawa, N. Polarized Infrared Absorbance Spectra of an Optically Anisotropic Crystal: Application to the Orientation of the OH^- Dipole in Quartz. *Phys. Chem. Minerals* **1993**, *20*, 308-314.

22. Leftin, A.; Molugu, Trivikram R.; Job, C.; Beyer, K.; Brown, Michael F. Area Per Lipid and Cholesterol Interactions in Membranes from Separated Local-Field ^{13}C NMR Spectroscopy. *Biophys. J.* **2014**, *107*, 2274-2286.

23. Tolstoy, V. P.; Chernyshova, I.; Skryshevsky, V. A. *Handbook of Infrared Spectroscopy of Ultrathin Films;* John Wiley & Sons, Hoboken, New Jersey, U.S.A., 2003.

24. Li, Y.; Ishida, H., Concentration-Dependent Conformation of Alkyl Tail in the Nanoconfined Space: Hexadecylamine in the Silicate Galleries. *Langmuir* **2003**, *19*, 2479-2484.

25. Benítez, J. J.; San-Miguel, M. A.; Domínguez-Meister, S.; Heredia-Guerrero, J. A.; Salmeron, M., Structure and Chemical State of Octadecylamine Self-Assembled Monolayers on Mica. *J. Phys. Chem. C* **2011**, *115*, 19716-19723.

26. Ida, N.; Tani, J.; Domae, M. Optimal Condition for Film-Forming Amine Treatment on Carbon Steel Effects of Film-Forming Amine Concentration and Temperature on Film Properties. *CRIEPI Report*, Q19011, 2020, https://criepi.denken.or.jp/jp/kenkikaku/report/detail/Q19011.html (accessed Mar 2, 2022).

27. Pan, L.; Zhu, X.-D.; Xie, X.-M.; Liu, Y.-T. Delicate Ternary Heterostructures Achieved by Hierarchical Co-Assembly of Ag and Fe_3O_4 Nanoparticles on MoS_2 Nanosheets: Morphological and Compositional Synergy in Reversible Lithium Storage. *J. Mater. Chem. A* **2015**, *3*, 2726-2733.

28. Jeffrey, G. A. *An Introduction to Hydrogen Bonding;* Oxford University Press: New York, U. S. A., 1997.

29. Hasegawa, T. *Quantitative Infrared Spectroscopy for Understanding of a Condensed Matter;* Springer: Tokyo, Japan, 2017.

30. Hasegawa, T.; Shioya, N. MAIRS: Innovation of Molecular Orientation Analysis in a Thin Film. *Bull. Chem. Soc. Jpn.* **2020**, *93*, 1127-1138.

31. Swift, A. J. Surface Analysis of Corrosion Inhibitor Films by XPS and ToFSIMS. *Mikrochim. Acta* **1995**, *120*, 149-158.

32. Hernández, M. P.; Fernández-Bertrán, J. F.; Farías, M. H.; Díaz, J. A. Reaction of Imidazole in Gas Phase at Very Low Pressure with Cu Foil and Cu Oxides Studied by X-Ray Photoelectron Spectroscopy. *Surf. Interface Anal.* **2007**, 39, 434-437.

33. Ederer, J.; Janoš, P.; Ecorchard, P.; Tolasz, J.; Štengl, V.; Beneš, H.; Perchacz, M.; Pop-Georgievski, O. Determination of Amino Groups on Functionalized Graphene Oxide for Polyurethane Nanomaterials: XPS Quantitation Vs. Functional Speciation. *RSC Adv.* **2017**, *7*, 12464-12473.

34. Biesinger, M. C. Advanced Analysis of Copper X-Ray Photoelectron *Spectra. Surf. Interface Anal.* **2017**, *49*, 1325-1334.

35. Jiang, P.; Prendergast, D.; Borondics, F.; Porsgaard, S.; Giovanetti, L.; Pach, E.; Newberg, J.; Bluhm, H.; Besenbacher, F.; Salmeron, M. Experimental and Theoretical Investigation of the Electronic Structure of Cu_2O and CuO Thin Films on Cu(110) Using X-Ray Photoelectron and Absorption Spectroscopy. *J. Chem. Phys.* **2013**, *138*, 024704.

36. Yamamoto, S.; Bluhm, H.; Andersson, K.; Ketteler, G.; Ogasawara, H.; Salmeron, M.; Nilsson, A. In Situ X-Ray Photoelectron Spectroscopy Studies of Water on Metals and Oxides at Ambient Conditions. *J. Phys. Condens. Matter* **2008**, *20*, 184025.

37. Wang, Y.; Lü, Y.; Zhan, W.; Xie, Z.; Kuang, Q.; Zheng, L. Synthesis of Porous Cu_2O/CuO Cages Using Cu-Based Metal–Organic Frameworks as Templates and Their Gas-Sensing Properties. *J. Mater. Chem. A* **2015**, *3*, 12796-12803.

38. Varadwaj, G. B. B.; Rana, S.; Parida, K. M. A Stable Amine Functionalized Montmorillonite Supported Cu, Ni Catalyst Showing Synergistic and Co-Operative Effectiveness Towards C–S Coupling Reactions. *RSC Adv.* **2013**, *3*, 7570-7578.

39. Ling, C.; Liu, F.-Q.; Xu, C.; Chen, T.-P.; Li, A.-M. An Integrative Technique Based on Synergistic Coremoval and Sequential Recovery of Copper and Tetracycline with Dual-Functional Chelating Resin: Roles of Amine and Carboxyl Groups. *ACS Appl. Mater. Interfaces* **2013**, *5*, 11808-11817.

40. Zhang, X.; Jiang, X.; Zhu, X.; Kong, X. Z. Effective Enhancement of Cu Ions Adsorption on Porous Polyurea Adsorbent by Carboxylic Modification of Its Terminal Amine Groups. *React. Funct. Polym.* **2020**, *147*, 104450.

41. Giordani, C.; Wakai, C.; Okamura, E.; Matubayasi, N.; Nakahara, M. Dynamic and 2d Nmr Studies on Hydrogen-Bonding Aggregates of Cholesterol in Low-Polarity Organic Solvents. *J. Phys. Chem. B* **2006**, *110*, 15205-15211.

42. Topp, H.; Steinbrecht, D.; Hater, W.; Giulini, B.; de Bache, A. The Influence of Film-Forming Amines on Heat Transfer During Saturated Pool Boiling. *PowerPlant Chem.* **2010**, *12*, 388-395.

43. Mori, S.; Ujiie, S.; Koizumi, M.; Uchida, K.; Lin, Q. IWC 20-26: FFS as a Heat Transfer Efficiency Improver for Steam Facilities. *Proceedings of the 81st Annual International Water Conference*, **2020** (Virtual conference).

TOC Graphic